Neutron and heavy-ion induced reactions using ^{204,208}Pb targets.

A thesis submitted in partial fulfilment of the requirements for the award of degree of

Master of Science

In

Physics

Submitted by:

AMANDEEP KAUR
Roll No. 301004001

Under the guidance of

Mr. MANOJ K. SHARMA
Associate Professor
SPMS,
Thapar University, Patiala.

School of Physics and Material Science,

Thapar University,
(Formerly Thapar Institute of Engineering and Technology)
Patiala-147004, INDIA

July-2012

"Our paths may change as life goes along, but the bond between us remains ever strong."

I lovingly dedicate this thesis to my brother GAURAVDEEP SINGH, who has always been supportive towards me.

CERTIFICATE

I hereby certify that the work which has been presented in this thesis entitled, "**Neutron and heavy-ion induced reactions using ^{204,208}Pb targets.**" submitted in partial fulfilment of the requirements for the award of degree of **Master of Science** in **Physics** at **Thapar University, Patiala**, is an authentic record of my own work carried out under the supervision of Mr. **Manoj K. Sharma, Associate Professor, SPMS** and refers other researcher's work which are duly listed in reference section.

The matter embodied in this thesis has not been submitted for the award of any other degree of this or any other university.

Amandeep Kaur

(Amandeep Kaur)

Date: 15/7/12

This is to certify that the above statement made by the candidate is correct and true to best of my knowledge.

Mr. Manoj K. Sharma
Associate Professor,
SPMS
Thapar University,
Patiala.

Counter signed by

Dr. Kulvir Singh
Associate Professor and Head,
School of Physics and Material Science,
Thapar University,
Patiala-147004

Dr. S. K. Mohapatra,
Dean of Academic Affairs,
Thapar University,
Patiala-147004

pg. 3

ACKNOWLEDGMENT

With a deep sense of gratitude, I wish to express my sincere thanks to my supervisor, **Mr. Manoj K. Sharma, Associate Professor, SPMS,** for their immense help in planning and executing the work in time. "*A good teacher is like a candle- it consumes itself to light the way of others."* The confidence and dynamism with which **Mr. Manoj K. Sharma** guided the work requires no elaboration. His company and assurance at the time of crisis would be remembered life-long. His valuable suggestions as final words during the course of work are greatly acknowledged. What I know today about the process of research, I learned from **Mr. Manoj K. Sharma.** My sincere thanks to him for the help extended to me when I approached him and the valuable discussion that I had with him during the course of thesis.

I express my heartfelt gratefulness to **Ms. Kirandeep Sandhu, Ms. Gurvinder Kaur, Mrs. Manpreet Kaur** and **Ms. Gudveen Sawhney** for extending timely help in carrying out my important works. The co-operation I received from other faculty members of this department is gratefully acknowledged. I will be failing in my duty if I do not mention the laboratory staff and administrative staff of this department for their timely help.

Thank you, LORD, for always being there for me.

I also want to thank my friends Manjot Kaur, Rimi Singh, Malti Verma, Ramandeep Kaur Bhullar, Navjot Dhindsa, Simran and Navpreet Kaur for their support and with whom I created unforgettable memories during my thesis work. I also want to thank my family, who taught me the value of hard work by setting their own example. Special thanks to my uncle, Mr. Paramjit Singh, whose blessings and advices I will need throughout my life.

Finally, I would like to thank all those whose direct and indirect support helped me completing my thesis in time.

Date: **Amandeep Kaur**

Abstract

Dynamical cluster decay model (DCM) has been applied to study the dynamics of neutron induced reactions. The DCM based cross-sections for neutron induced reactions as well as heavy-ion induced reactions agree fairly with experimental data. The following reactions are studied and worked upon over a wide range (14-21 MeV) of incident energies.

- ${}_{0}^{1}n + {}_{82}^{208}Pb \rightarrow {}_{82}^{209}Pb* \rightarrow {}_{81}^{208}Tl + {}_{1}^{1}H$
- ${}_{0}^{1}n + {}_{82}^{204}Pb \rightarrow {}_{82}^{205}Pb* \rightarrow {}_{82}^{203}Pb + 2{}_{0}^{1}n$
- ${}_{10}^{20}Ne + {}_{82}^{208}Pb \rightarrow {}_{92}^{228}U* \rightarrow fission\ fragments$

This dissertation comprises of three chapters.

Chapter-1:

Chapter-1 consists of the basic over-view of neutron induced reactions, neutron sources, neutron cross-sections and various types of neutron interactions with target nucleus.

Chapter-2:

Chapter-2 consists of the description of dynamical cluster decay model (DCM). It gives description about the various potentials used in DCM along with other parameters of the model. The deformation effects of nuclear systems are included in the framework of DCM.

Chapter-3:

Chapter-3 consists of the details of the DCM based calculations for the above mentioned reactions.

Contents

List of figures:

Chapter-1

Chapter-2

Chapter-3

Fig. 3.5 Variation of fragmentation potential, V_η with fragment mass A_2 for $^{208}Pb(n,2n)^{207}Pb$ and $^{204}Pb(n,2n)^{203}Pb$ reaction at E_{cm}=20.29 MeV.

Fig. 3.6 Variation of preformation probability, P_0 with fragment mass A_2 for $^{208}Pb(n,2n)^{207}Pb$ and $^{204}Pb(n,2n)^{203}Pb$ reaction at E_{cm}=20.29 MeV.

Fig. 3.7 DCM based cross-sections and experimental data for (n,p) reactions of ^{208}Pb.

Fig. 3.8 (a) Fragmentation potential, Vη and **(b)** preformation probability, P_0 as a function of fragment mass, A_2 for $^{20}Ne + ^{208}Pb$ reaction.

List of tables:

Chapter-1

Chapter-3

CHAPTER-1

Literature survey

1.1 Introduction:

Neutron induced fusion has been a field of intense study in past few decades [1-6]. This study mainly deals with the light charged particle production such as (n,p), (n,n), (n,2n) and (n,3n). During the last decades, many groups have been involved in the theoretical and experimental studies of light charged particle production in neutron-induced reactions using different targets. The (n,p), (n,n), (n,2n), (n,3n) and (n,α) reactions have specific features due to the rather low intensity of the incident neutron beam giving rise to fairly low reaction cross-sections [7]. The activation cross-sections for various processes like $^{46}Ti(n,p)^{46}Sc$, $^{60}Ni(n,p)^{60}Co$, $^{76}Ge(n,2n)^{75}Ge$, $^{59}Co(n,2n)^{58}Co$ etc are studied experimentally [1-6]. Particularly, the isotopes of lead are used in experimental as well as theoretical studies because of the double shell closure of ^{208}Pb and we have a large number of stable isotopes for various nuclear studies for Z=82 [8].

A neutron is one of the fundamental particles that make up matter. This uncharged particle exists in the nucleus of a typical atom, along with its positively charged counterpart, the proton. Protons and neutrons each have about the same mass, and both can exist as free particles away from the nucleus. In the universe, neutrons are abundant, making up more than half of all visible matter. Neutrons have many properties that make them ideal for carrying out research in the areas of nuclear physics. Because of their unique sensitivity to hydrogen, neutrons can be used to precisely locate hydrogen atoms, enabling a more accurate determination of molecular structure, which is important for the design of new drugs. Neutrons scattered from hydrogen in water can locate moisture in fighter jet wings that leads to corrosion and helps in identifying the part of wing which needed replacement. Atomic model of yttrium-barium-copper oxide, a superconducting ceramic whose oxygen positions are determined by neutron scattering. This capability allowed scientists to determine the critical positions of light oxygen atoms in yttrium-barium-copper oxide (YBCO), a very good high-temperature and superconducting ceramic. The major properties of neutrons are:

Neutrons are neutral particles. They are highly penetrating and interact through short range nuclear forces and do not destroy the sample. Neutrons have a magnetic moment. They can be used to study microscopic magnetic structure, study magnetic fluctuations and to develop magnetic materials. Neutrons have spin. They can be formed into polarized neutron beams to study nuclear (atomic) orientation and are used in coherent and incoherent scattering. The energies of thermal neutrons are similar to the energies of elementary excitations in solids.

Both have similar molecular vibrations, lattice modes and dynamics of atomic motion. The wavelengths of neutrons are similar to atomic spacing hence they can determine structural sensitivity, structural information from 10^{-13} to 10^{-4} cm and crystal structures. Neutrons are used to investigate nuclear behaviour. They are sensitive to light atoms, can exploit isotopic substitution and can be used to differentiate complex molecular structures.

1.2 Why do we need neutron induced reactions:-

The study of neutron-induced reactions is of large importance in a wide variety of research fields, ranging from stellar nucleo-synthesis, symmetry breaking effects in compound nuclei, and the investigation of nuclear level densities, to applications of nuclear technology. Most of the experiments are concerning with neutron-induced fission and neutron capture measurements. The neutrons incident on the nuclei produce reaction product, fission fragments or gamma rays, which are then detected with dedicated particle detectors. Neutron cross-section measurements are important for the fields of fundamental and applied nuclear physics. The most important ones have always been nuclear astrophysics and nuclear technology, but neutron data are also important in nuclear medicine, for material science, for archaeological and cultural studies, etc. In fundamental nuclear physics, neutrons have always been a precious probe to investigate the structure of nuclei, and the nature of fundamental forces.

1.3 How can the demand for neutrons be met:-

Most of today's neutron sources are based on nuclear reactors; additionally there are a number of accelerator-based sources which produce neutrons by the nuclear spallation process. Most of the reactor sources were built in the 1950s and 1960s, and have come to the end of their useful lives. In fact between the years 2010 and 2020 the 1st generation capacity of neutron sources for beam research will decrease drastically. However, some new reactions are coming up and hence the neutron flux can be accordingly optimised. The most important class of new-generation sources consists of the accelerator-based spallation facilities, whose increased power will lead to improvements in the quantity and quality of research, and enable expansion into new scientific areas. At present a number of specific projects are in the planning and developing stage in Europe, Austria, North America, Japan and India. Neutrons can be produced from neutron sources such as nuclear reactors, radio-isotopes, or accelerator based sources. A nuclear reactor is the most inexhaustible source for the production of neutrons of all energies. However, the complexity of a reactor and the systems involved as

well as the cost make simple and broad use of reactors. On the other hand, radioisotope neutron sources are used in an innumerable amount of industrial applications and are ideal when a continuous source is needed. However, such a source is not appropriate for purposes that require neutrons of specific energy [8].

Small scale accelerators and compact pulse neutron sources use nuclear reactions to produce neutrons. The most common are deuterium-deuterium (^{2}H-^{2}H) and deuterium-tritium (^{2}H-^{3}H) reactions.

$$^{3}\text{H}\ (^{2}\text{H,n})\ ^{4}\text{He} \qquad Q = 17.59\ MeV$$

$$^{2}\text{H}\ (^{2}\text{H,n})\ ^{3}\text{He} \qquad Q = 3.27\ MeV$$

These reactions produce 14.1 MeV and 2.5 MeV neutrons respectively.

1.4 Classification of neutrons:-

Neutrons are classified according to their energies because their interaction with matter is energy dependent. The most common classification is:-

Table 1.1 Classification of neutrons on the basis of their energy.

Neutron energy	Name
0-0.025eV	Cold
0.025eV	Thermal
0.025eV-0.4eV	Epithermal
0.4eV-0.6eV	Cadmium
0.6eV-1eV	Epicadmium
1eV-10eV	Slow
10eV-300eV	Resonance
300eV-1MeV	Intermediate
1MeV-20MeV	Fast
>20MeV	Relativistic

Since in the presence work we intend to work in energy range 14 MeV to 21 MeV so our main focus will be to deal with interaction criteria of fast neutron for some stable targets like that of ^{204}Pb and ^{208}Pb.

1.5 Concept of Nuclear cross-section:-

When a beam of particles is incident upon a target nucleus, it interacts with the target either through scattering or absorption and thus its energy or intensity gets attenuated. Each nucleus has an associated area σ in a direction perpendicular to the incident beam such that if the centre of the incident particle lies within that area then only the reaction will take place otherwise not. This effective area, σ is a measure of the probability of occurrence of a particular reaction. Thus, *the probability of occurrence of a particular nuclear reaction is described by the effective cross-section of a nucleus for that reaction.* The cross-section may also be defined as:

1) The probability that a reaction will take place when a single nucleus is incident upon by a beam of particles of flux one particle per unit area.
2) The probability that the reaction will take place when a single particle is shot perpendicular at a target nucleus consisting of one nucleus per unit area.

Now, when a projectile is incident on a target nucleus, there are two possibilities. Either that incident particle bounces off i.e. scatters away from the target nuclei or it disappears after the reaction i.e. it is absorbed by the nucleus. Therefore, when we calculate the reaction cross-sections for any nuclear reactions, it will be a sum of the scattering cross-sections (σ_s) and absorption cross-sections (σ_a). Thus, the total cross-section is written as:

$$\sigma_T = \sigma_S + \sigma_A$$

The various types of nuclear cross-sections are:

1.) Total reaction cross-section, σ_T: This detects the reaction products scattering in a region of 4π.

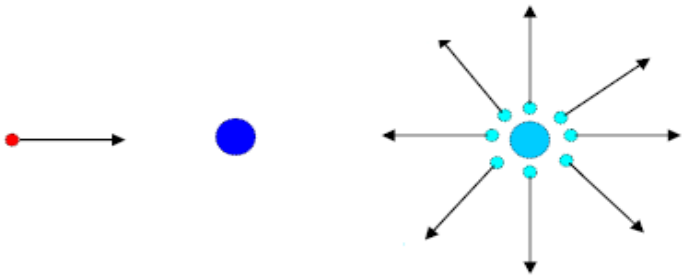

Fig. 1.1 Fragments scattering in a solid angle of 4π.

2.) Differential cross-section, $\frac{d\sigma}{d\Omega}$: It detects angular distribution of the fragments. This measures the reaction products emitted at an angle θ within a solid angle dΩ.

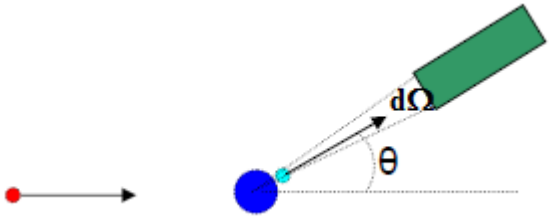

Fig.1. 2 Reaction products scattered at an angle θ within solid angle dΩ.

The unit assigned for measuring nuclear cross-sections is *barn*, where $1\ barn = 10^{-28} m^2$

1.6 Neutron interactions:

The interaction of neutron with matter depends upon the energy which the neutron carries. More the energy carried by the incident neutron, more strong is its interaction with the matter. The interaction of a neutron with matter is broadly classified as of two types:

- Absorption
- Scattering

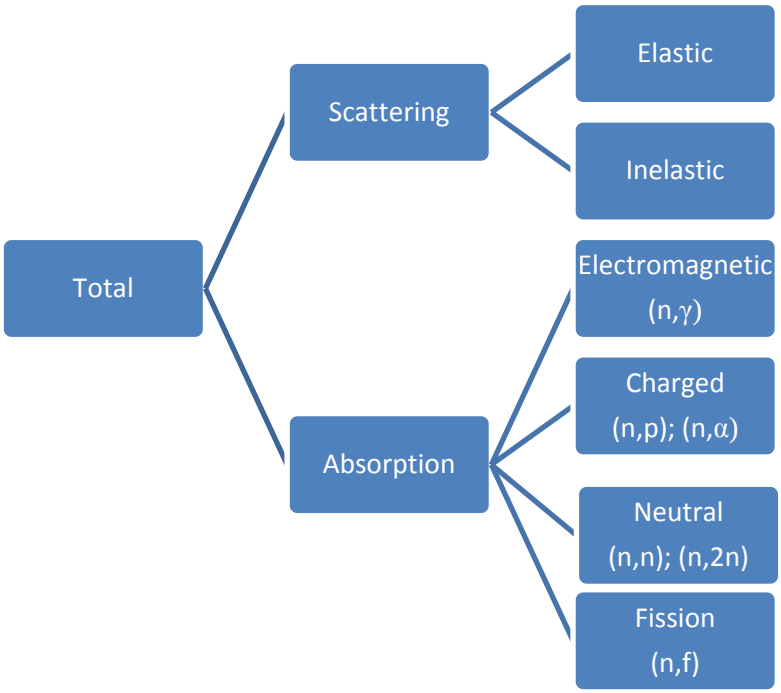

Fig. 1.3 Various categories of neutron interactions.

When a neutron is scattered, its speed and direction changes but there is no change in the state of the target nucleus i.e. it does not lose its identity. On the other hand, when a neutron is absorbed, a large number of radiations can be emitted and it may lead to fission of nucleus.

Basically, neutron interactions can be described in three steps:

- The condition before the interaction when neutron is approaching the nucleus.
- An intermediate stage when the neutron forms a compound nucleus with the target.
- And the condition after the interaction.

In the intermediate stage the neutron is incorporated into the target nucleus and forms a compound nucleus that has atomic mass increased by 1 unit as compared to the parent nucleus. The formation of compuond nucleus means that the neutron has transferred its energy to the target nucleus. A compound nucleus is highly unstable and decays within a time period of approx. 10^{-15} seconds.

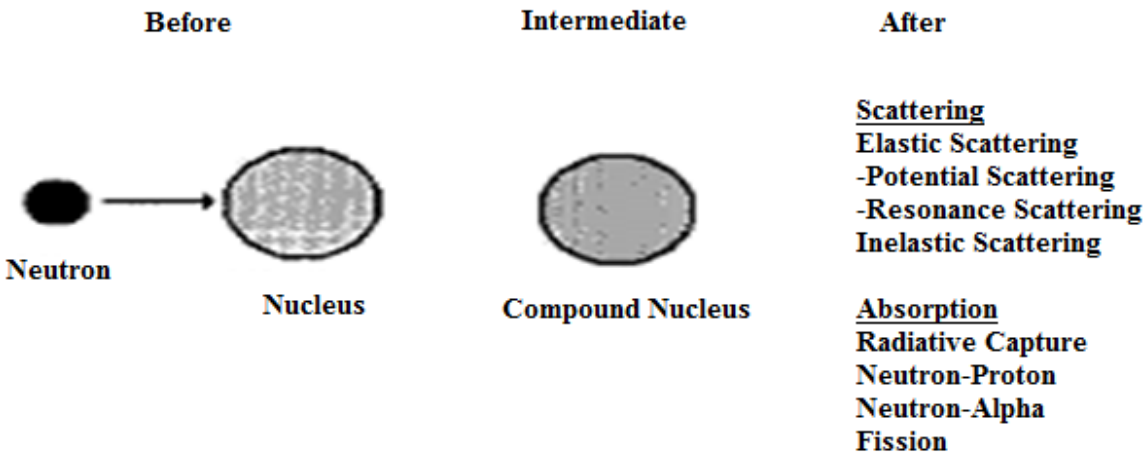

Fig.1.4 Neutron interaction in a three-way step i.e. before, intermediate and after the interaction of neutron.

One of the important and characteristic features of neutron interactions with matter is that the cross-sections exhibits maximum values at certain incident neutron energies. These maximum values are called *resonances.* An incident neutron and target nucleus is more likely to combine and form a compound nucleus if the energy of the incident neutron is such that the compound nucleus is produced in one of its excited states. These resonances appear in the cross-sections because it is necessary to form the compound nucleus before the interaction can proceed. The excitation energy of the compound nucleus is equal to the kinetic energy of the incident neutron plus the separation energy (binding energy) of the neutron in compound nucleus.

Compound nucleus:

Consider a region of space where the target nucleus in any excited state is enclosed. This domain is known as internal region and the remaining space is the external region. The surface is well defined by some nuclear shape. A nucleon hits this region and a compound nucleus is formed. An unbound state is obtained and the nucleus disintegrates after a mean life time of $\hbar/\Gamma$. The compound nucleus is created during a short period of time, enabling a redistribution of the kinetic energy and the momentum of the incoming particle among the entire system [9]. According to Bohr, the formation of this compound nucleus takes place in two distinct and independent stages: (i) formation of compound nucleus C, which survives a relatively longer time and (ii) the disintegration of the compound nucleus into the products of the reaction.

$$x + X \rightarrow C^*$$

The incident particle is captured by a target nucleus, gives up its energy to few nucleons and as the results of the interaction of these nucleons with all others, the energy is quickly distributed among all the nucleons of the target nucleus. The new nucleus thus formed is called *compound nucleus.* The mode of disintegration of compound nucleus ($C^* \rightarrow Y + y$) is independent of the mode of formation and depends on its energy, parity and angular momentum. A compound nucleus, once formed, can decay in a number of different ways, each with its own intrinsic probability. For ex. $^{27}Al^*$ can decay in number of ways. A few are shown here: $^{27}Al^* \rightarrow (^{23}Na + \alpha)$, $(^{25}Mg + p)$, $(^{26}Al + n)$ or $(^{27}Al + \gamma)$. The compound nucleus has a life time which is long (10^{-14} to 10^{-18} sec) as compared to the time for a nucleon to traverse a nucleus (10^{-20} to 10^{-23} sec).

A brief discussion of the neutron interactions can be done as follows:

1.6.1 Elastic scattering (n,n):

There are two possible ways for a neutron to scatter elastically from a nucleus:

- *Resonance or compound elastic scattering:* The neutron is absorbed by the target nucleus to form a compound nucleus followed by re-emission of neutron. In this scattering the initial and final states are same. The initial state moves to final state through an intermediate state. This intermediate state is formed by the absorption of incident neutrons by the target nucleus. The nucleus so formed is called *compound nucleus.* The compound nucleus thus formed is having same atomic number as that of parent nucleus but its mass number is increased by 1 unit.
- *Potential elastic scattering:* the neutron is scattered away from the nucleus by the short range nuclear force. Potential elastic scattering is more common and can be understood by visualizing neutron and nuclei as billiard balls with impenetrable surfaces. Potential scattering is that in which the neutron never actually touches the nucleus and compound nucleus is not formed. Such interactions take place with incident neutrons of energies up to about 1 MeV. Neutrons are scattered by the short range forces as they approach the nucleus. The cross-section is approximately constant and is given by the relation:

$$\sigma = 4\pi R^2$$; where R= radius of the nucleus.

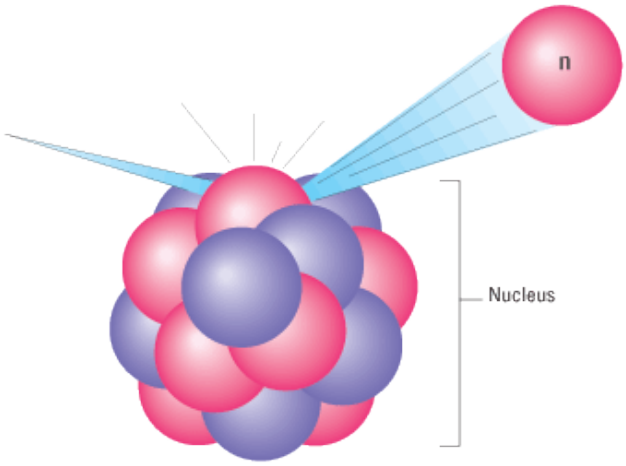

Fig.1.5 Shows elastic neutron scattering (courtesy: iramis.cea.fr).

An elastic scattering reaction between a neutron and the target nucleus does not involve any energy transfer into the nucleus. Momentum and kinetic energy are, however, conserved and usually there is a transfer of kinetic energy from the neutron to the target nucleus. The target nucleus thus gains the amount of kinetic energy that the neutron loses and moves away at an increased speed. If the neutron collides with a massive nucleus it rebounds with almost the same speed and loses a negligible amount of energy.

1.6.2 Inelastic scattering (n,n´):

In order for a neutron to undergo inelastic scattering with a nucleus its incident energy must to be sufficient to place the target nucleus in an excited state. As a result, inelastic scattering cross-section exhibit threshold energy. In general, the energy levels of the excited states of a nucleus decrease with increasing mass number. Elements with lower mass number have increased nuclear excitation energies. This is why neutron inelastic scattering is more probable for heavier nuclei and thus the inelastic cross-section is non-zero over a large energy region for heavier nuclei. At energies well above the threshold value, the inelastic cross-section is equal to the elastic cross-section. This scattering proceeds through two steps:

The compound nucleus formed is in excited state due to energy imparted to it due to incident neutron. In next step, a neutron of lower kinetic energy is expelled from the nucleus leaving the nucleus in lower excited state. The nucleus then regains its ground state by emitting the excess energy in the form of γ–ray.

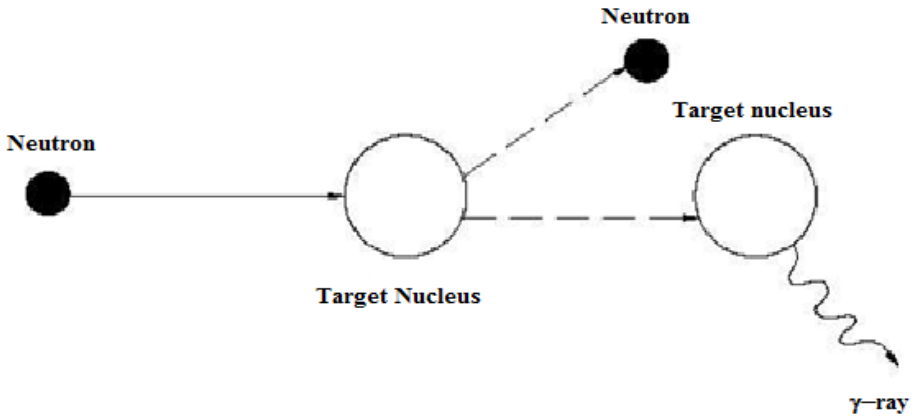

Fig.1.6 Shows inelastic neutron scattering from the target (courtesy:nuclearpowertraining.tpub.com).

1.6.3 Radiative capture (n,γ):

The radiative capture reaction proceeds through the formation of a compound nucleus and this compound nucleus subsequently decays by emitting one or several gamma rays. This reaction can be written as:

$(Z,A) + n \rightarrow (Z,A+1)^* \rightarrow (Z,A+1) + \gamma$

Neutron capture is often called radiative capture because gamma rays are mostly emitted in these reactions. The compound nucleus formed here is having mass number increased by one from the original nucleus. The newly formed nucleus can be radioactive and will therefore decay. The neutron capture reaction does not require any specific neutron energy and the reaction can occur at any neutron energy level. These reactions are mostly exothermic because the binding energy of the newly formed nucleus is larger than the sum of binding energies of the neutron and original nucleus.

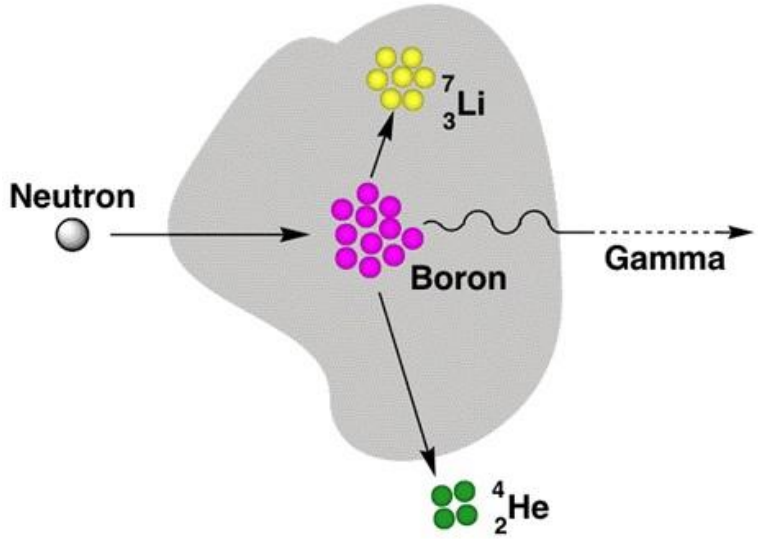

Fig.1.7 Schematics of radiative neutron capture (courtesy: wewantfullmarksforchemistry.blogspot.com)

The radiative capture cross-section is divided into three groups:

- In low-energy region, for most of the nuclei, the radiative capture cross-section varies as inverse square root of incident neutron energy. Since the neutron speed is proportional to the square root of energy, the radiative capture cross-section is said to vary as 1/v, where v is the velocity of the incident neutron. Thus cross-section will vary as inverse square root of incident neutron energy.
- Above 1/v region, one gets the resonance region with the energy range same as that for the elastic scattering. It is so because the nucleus formed in the radiative capture is identical to the compound nucleus formed in the elastic scattering. The radiative capture cross-section in resonance region is expressed by Breit-Wigner formula.
- Above the resonance region, the radiative capture cross-section drops rapidly and smoothly to very small values.

1.6.4 Charged particle emission (n,p) and (n,α):

The study of light charged particles (protons and α- particles) emitted in various neutron induced and heavy-ion induced reactions imparts quite interesting aspects related to nuclear structure and related phenomenon. The cross section of light particles is generally very large [10]. But this emission process of these light particles is rather complex. The light particles are emitted due to broadly three different processes namely compound, direct and pre-equilibrium which take place over different time scales. There are indications that they may

also be emitted during the formation stage of the compound nucleus. The light particles are influenced by the nuclear structure, nuclear mean field and dynamics of the collision. A charged particle reaction usually leads to emission of an α-particle or a proton from the nucleus. Thus charged particle reactions are usually rare with slow neutrons.

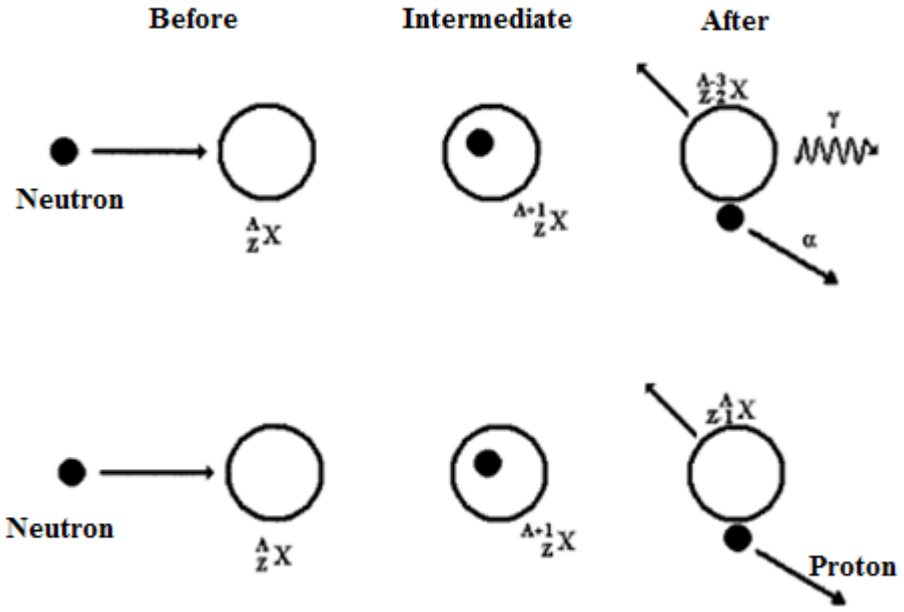

Fig.1.8 Schematics of charged particle emission.

Examples of these reactions are:

$$^{208}_{82}Pb + n \rightarrow {}^{209}_{82}Pb * \rightarrow {}^{208}_{81}Tl + p$$

$$^{10}_{5}B + n \rightarrow {}^{11}_{5}B * \rightarrow {}^{7}_{3}Li + \alpha$$

$$^{6}_{3}Li + n \rightarrow {}^{7}_{3}Li * \rightarrow {}^{3}_{1}H + \alpha$$

1.6.5 Neutron induced fission (n,f):

Neutron induced fission is the splitting of a heavier nucleus into two or more smaller fragments. The smaller fragments have large binding energies as compared to the larger fragment. Thus, neutron induced fissions are always accompanied by the emission of enormous amount of heat/energy. The by-products may be neutron, protons, α-particles etc. which may be helpful in starting a chain reaction.

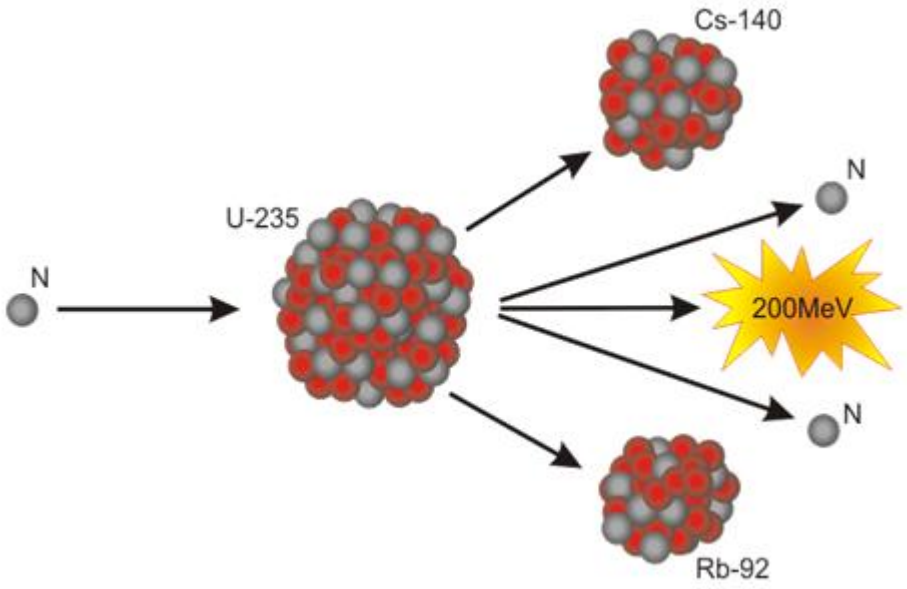

Fig.1.9 Neutron induced fission reaction (n,f) (courtesy: www.sciencebuzz.org).

This is how neutrons can be utilised for studying various reaction dynamics using stable target nuclei. Formerly in the study of nuclear reactions, the projectiles used were basically the neutrons or alpha particles from natural radioactive substances. Low energy neutrons can easily penetrate coulomb barrier and cause nuclear reactions. Later on, the advent of highly advanced particle accelerators techniques has made possible the high energy beams of not only protons, deuterons and alpha particles but also of heavy ions, to produce nuclear reactions. Highly efficient and precise detector technology, to observe nuclear phenomena, is available. Fast computational methods further aided in precise and accurate measurements of cross sections and angular distribution of the disintegration products in the experiments. As a result, lot of experimental data related to different nuclear phenomena have become available. Nuclear reactions induced by heavy ions have become the principal tool in nuclear physics research. We can also use heavier nuclei to induce such reactions which help us in carrying out certain investigations which are useful to explore some important features related to nuclear structure and nuclear reactions. Those nuclei whose mass number is greater than alpha-particle constitute the category of heavy-ions. And nuclear reactions carried out by such projectiles are called *heavy-ion induced reactions.* In the past over two-decades, heavy-ions are used as projectiles to study the fission of compound nucleus for a wide range of fissility Z^2/A, excitation energy and angular momentum. They are helpful in studying fission of various stable and unstable heavy nuclei.

In the present work, the heavy-ion induced fission of ^{208}Pb using ^{20}Ne as projectile is investigated. The decay of compound nucleus thus formed ($^{228}U^{*}$) is studied at low excitation energies [11]. The compound nuclei (CN) formed in low-energy heavy-ion reactions are highly excited and carry large angular momentum. The compound systems so formed may also emit multiple light particles, LPs (n, p, α) and γ-rays along with fission products. In this work, we have carried out extensive theoretical study on (n,p), (n,2n) and heavy-ion induced fission reactions using ^{204}Pb and ^{208}Pb targets over a wide range of incident energies. For the purpose we have used dynamical cluster decay model (DCM) [12-16] which is used successfully for a variety of nuclear reactions during last one decade.

1.7 References:

1. I. G. Birn, B. Strohmaier, H. Freiesleben and S. M. Qaim, Phys. Rev. C 52, 5 (1995).
2. S. Suda'r and S. M. Qaim, Phys. Rev. C 53, 6 (1996).
3. C. D. Nesraja, S. Suda'r and S. M. Qaim, Phys. Rev. C. 68, 024603 (2003).
4. M. Al-Abyad, S. Suda'r M. N. H. Comsan and S. M. Qaim, Phys. Rev. C 73, 064608 (2006).
5. F. Cserpa'k, S. Suda'r, J. Csikai and S. M. Qaim, Phys. Rev. C. 49, 3 (1994).
6. N. I. Molla and S. M. Qaim, Phys. Rev. C. 42, 4 (1990).
7. J. P. Meulders et.al Pramana J. of Phys. Vol. 57, No. 1 pp.85-95 (2001).
8. V. Semkova et.al Phys. Rev. C, Vol.80, 024610 (2009).
9. Emil Petrescu, Mihail Mirea, U. P. B. Sci. Bull Series A, Vol. 70, No. 3 pp.59-72 (2008).
10. S Kailas, Pramana J. of Phys. Vol 57, No. 1 pp.75-84 (2001).
11. R. Tripathi, K. Sudarshan *etal.* Phys. Rev. C, Vol.69, 024613 (2004).
12. R. K. Gupta, S. K. Arun, R. Kumar and Niyti Int. Rev. Phys. (IREPHY) **2** 369 (2008).
13. B. B. Singh, M. K. Sharma and R. K. Gupta, Phys. Rev. C **77** 054613 (2008).
14. M. K. Sharma, G. Sawhney, R. K. Gupta and W. Greiner, J. Phys. G: Nucl. Part. Phys. **38** 105101 (13pp) (2011); M. K. Sharma, G. Sawhney, S. Kanwar and R. K. Gupta, Mod. Phys. Lett. A vol. **25**, No.s 21-23 2022-2023 (2010).
15. K. Sandhu, M. K. Sharma and R. K. Gupta, Phys. Rev. C **85** 024604 (2012).
16. M. Kaur, R. Kumar and M. K. Sharma Phys. Rev. C **85** 014609 (2012); M. Kaur, M. K. Sharma Phys. Rev. C **85** 054605 (2012).

CHAPTER-2

The DCM Model:

2.1 Features of DCM [1]-[9]

DCM is used to study heavy ion reaction dynamics especially the decay of excited compound nucleus. In this model, deformation and orientation effects of the reaction partners and decay products are explicitly included along with temperature and angular momentum contributions. DCM is applied to study various mass regions which can be categorised on the basis of their mass numbers as light mass ($^{48}Cr^{*}$, $^{56}Ni^{*}$), intermediate mass ($^{116,118,122}Ba^{*}$, $^{164}Yb^{*}$), heavy ($^{176\text{-}196}Pt^{*}$, $^{201}Bi^{*}$, $^{202}Pb^{*}$, $^{204}Po^{*}$, $^{217}Fr^{*}$, $^{219,220}Ra^{*}$, $^{246}Bk^{*}$) and super-heavy ($^{286}112^{*}$, $^{286}114^{*}$, $^{297}117^{*}$)

The DCM, worked out in terms of the collective coordinates of mass asymmetry $\eta = \frac{A_1 - A_2}{A_1 + A_2}$ and relative separation R respectively gives:

a) The nucleon-division (or exchange) between the outgoing fragments.

b) Transfer of kinetic energy of incident channel (E_{CM}) to internal excitation (total excitation or total kinetic energy, TXE or TKE) of the outgoing channel. It may be noted that the fixed decay point R = R_a (defined later) at which the process is calculated, depends upon temperature T as well as on η (i.e. (T, η)). This energy transfer process can be calculated as follows with the help of

$$E^{*}_{CN} = E_{c.m} + Q_{in=} \left| Qout \right| + TKE(T) + TXE(T) \quad (2.1)$$

The CN excitation E^{*}_{CN} is related to temperature T (in MeV) and is given by:

$$E^{*}_{CN} = \frac{A}{a}T^{2} - T\ (MeV); \quad (2.2)$$

where $\frac{A}{a}$ *is level density parameter with* $'a'$ *in the range* 9 *to* 12.

As we have taken different values of 'a' i.e. a=9, 10, 11 and 12 for (n,p) reaction and a=12 for (n,2n) and (n,f) reactions, so for practical use 'a' is termed as level density parameter in calculations of chapter-3.

This model is a two-step model:

a) First step is quantum mechanical preformation probability P_0 of the decay products or cluster formed in the mother nuclei.

b) Second step is the penetration of the fragments/ clusters through the interaction barrier.

These two quantities are used to calculate the fusion-fission cross-sections:

$$\sigma = \frac{\pi}{k^2}\sum_{\ell=0}^{\ell_{max}}(2l+1)P_0P \tag{2.3}$$

with $k = \sqrt{\frac{2\mu E_{cm}}{\hbar^2}}$ and $\mu = \frac{A1A2}{A1+A2}m$, as reduced mass (and m is the nucleon mass).

Preformation probability refers to the motion in mass asymmetry coordinate $\eta = \frac{A_1 - A_2}{A_1 + A_2}$; (1 and 2 being heavy and light fragments) and the penetrability P to relative separation R motion. Both preformation probability and the penetrability depend on ℓ and T of the system, and on deformations $\beta_{\lambda i}$ and orientations θ_i of the two nuclei or fragments. (λ=2, 3, 4, for quadrupole, octupole, hexadecapole deformations)

2.2 Preformation probability,P_o:

The structure information of the CN enters the model via preformation probability P_o (also known as spectroscopic factor) of the fragments given by the solution of stationary Schrodinger equation in η which is given below:

$$H = \frac{-\hbar^2}{2\sqrt{B_{\eta\eta}}}\frac{\partial}{\partial_\eta}\frac{1}{\sqrt{B_{\eta\eta}}}\frac{\partial}{\partial_\eta} - \frac{\hbar^2}{2\sqrt{B_{RR}}}\frac{\partial}{\partial_R}\frac{1}{\sqrt{B_{RR}}}\frac{\partial}{\partial_R} + V(\eta) + V(R) \tag{2.4}$$

Schrodinger wave equation can be separated for the two co-ordinates η and R as follows,

$$\left[\frac{-\hbar^2}{2\sqrt{B_{\eta\eta}}}\frac{\partial}{\partial_\eta}\frac{1}{\sqrt{B_{\eta\eta}}}\frac{\partial}{\partial_\eta} + V(\eta)\right]\Psi^{\upsilon}(\eta) = E_\eta^{\upsilon}\Psi^{\upsilon}(\eta) \tag{2.5}$$

$$\left[\frac{-\hbar^2}{2\sqrt{B_{RR}}}\frac{\partial}{\partial_R}\frac{1}{\sqrt{B_{RR}}}\frac{\partial}{\partial_R} + V(R)\right]\Psi^{\upsilon}(\mathrm{R}) = E_R^{\upsilon}\Psi^{\upsilon}(\mathrm{R}) \tag{2.6}$$

With ψ (η, R) = ψ (η) ψ(R)

$E = E_\eta + E_R$

The states $\Psi^{\upsilon}s$ (η) are the vibrational states in the potential V (η) and are labelled by the quantum numbers ν =0, 1, 2……

The preformation probability is calculated by using

$P_0 \propto |\psi^0(\eta)|^2$.

The potential used in this Schrodinger equation is given by:

$$V_R(\eta,T)=\sum_{i=1}^{2}[V_{LDM}(A_i,Z_i,T)]+\sum_{i=1}^{2}[\delta U_i]\exp(-T^2/T_0^2)+V_c(R,Z_i,\beta_{\lambda i},\theta_i,T) \\ +V_P(R,A_i,\beta_{\lambda i},\theta_i,T)+V_\ell(R,A_i,\beta_{\lambda i},\theta_i,T) \quad (2.7)$$

where the T-dependent terms V_c, V_P and V_l are defined as follows: V_c is the Coulomb potential, V_P is the proximity potential for hot deformed nuclei and V_l is the potential due to rotational motion of hot deformed nuclei.

Further, in Eq. (2.7), within the Strutinsky renormalization procedure, one can define the binding energy B of a nucleus at temperature T as the sum of liquid drop energy V_{LDM} (T) and shell correction δU (T) i.e.

$$B(T)=V_{LDM}(T)+\delta U\exp(\frac{-T^2}{T_0^2}) \quad (2.8)$$

The T dependent liquid drop part of the binding energy V_{LDM} (T) is calculated from Davidson et al. [10], based on the semi-empirical mass formula of Seeger [11]. For the shell correction δU in Eq. (2.8), since there is no microscopic shell model known which gives the shell corrections for light nuclei, we use the empirical formula of Myers and Swiatecki [12].

The first two terms in the equation (2.7) represent the binding energy of the nucleus and is denoted as the sum of liquid drop energy V_{LDM} and shell correction δU(T) by equation (2.8).

2.3 Types of potentials:

The remaining three terms in eq. (2.7) can be explained as follows:

2.3.1 Coulomb potential:

The coulomb potential describes the force of repulsion between two interacting nuclei due to their charges. It acts along the line joining the two nuclei. The Coulomb potential for two interacting spherical nuclei is given as:

$$V_C = Z_1Z_2e^2/R$$

For interacting deformed and oriented nuclei, different authors [13]-[17] have derived it differently.

The Coulomb potential for hot and rotating, deformed and oriented nuclei given as:

$$V_c(Z_i, \beta_{\lambda i}, \theta_i, T) = \frac{Z_1 Z_2 e^2}{R(T)} + 3Z_1 Z_2 e^2 \sum_{\lambda, i=1,2} \frac{R_i^{\lambda}(d_i, T)}{(2\lambda+1)R(T)^{\lambda+1}} \quad (2.9)$$

2.3.2 The Proximity Potential for deformed, oriented and coplanar nuclei:

When two surfaces approach each other within a small distance of less than ~ 2fm, comparable with the surface thickness of interacting nuclei, or when a nucleus is at the verge of dividing into two fragments, then the two surfaces actually face each other across a small gap or crevice. In both cases, the surface energy term alone could not give rise to the strong attraction that is observed when the two surfaces are brought in close proximity. Such additional attractive forces are called proximity forces and corresponding potential is termed as nuclear proximity potential.

Blocki et al. [18] have reanalysed and extended a theorem, originally formed by Deryagin [19], according to which the force between two gently curved surfaces in close proximity is proportional to the interaction potential per unit area between the two flat surfaces. The original expression of Blocki based on the pocket formula was for spherical nuclei, and is given as

$$V_P(s_0) = 4\pi \overline{R} \gamma b \Phi(s_0). \quad (2.10)$$

$\Phi(s_0)$ is the universal function, independent of the shapes of nuclei or the geometry of nuclear system, but depends on the minimum separation distance

$$\Phi(s_0) = \begin{cases} -\frac{1}{2(s_0 - 2.54)}^2 - (s_0 - 2.54)^3 \\ -3.437 \exp\left(-\frac{s_0}{0.75}\right) \end{cases} \quad (2.11)$$

respectively, for $s_0 \leq 1.2511$ and $s_0 \geq 1.2511$. Here, s_0 is defined in units of b, i.e. s_0 is s_0/b. This function is defined for negative (the overlap region), zero (touching configuration) and positive values of s_0. For a fixed R, the minimum distance s_0 for spherical nuclei is defined as

$$s_0 = R - R_1 - R_2$$

2.3.3 Rotational Energy due to angular momentum:

The rotational motion gives an additional energy due to the angular momentum defined as

$$V_\ell(T) = \frac{\hbar^2 \ell(\ell+1)}{2I(T)} \tag{2.12}$$

with $I = \mu R^2$, is the non-sticking limit of moment of inertia with as the $\mu = \frac{A1A2}{A1+A2} m$ reduced mass m is the nucleon mass. In the complete sticking limit, the moment of inertia (I) is given as,

$$I = \mu R^2 + 2/5 A_1 m R_1^2 + 2/5 A_2 m R_2^2 \tag{2.13}$$

It is relative to mention here that value of angular momentum extracted experimentally, is based upon moment of inertia limit.

2.4 Penetration Probability P:

Penetrability P measures the capability of fragment nucleus to penetrate the potential barrier generalized during compound nucleus formation. The penetrability P is the WKB integral between R_a and R_b.

$$P = \exp\left[\frac{-2}{h} \int_{Ra}^{Rb} \{2\mu[V(R) - Qeff]^{\frac{1}{2}} dR\}\right] \tag{2.14}$$

Here first turning point is given as:

$$R_a = R_t + \Delta R(T) \tag{2.15}$$

where $Rt = R_1 + R_2$ (shown in fig. 2.1) (2.16)

ΔR (T) is the neck length parameter that assimilates the neck formation effects.

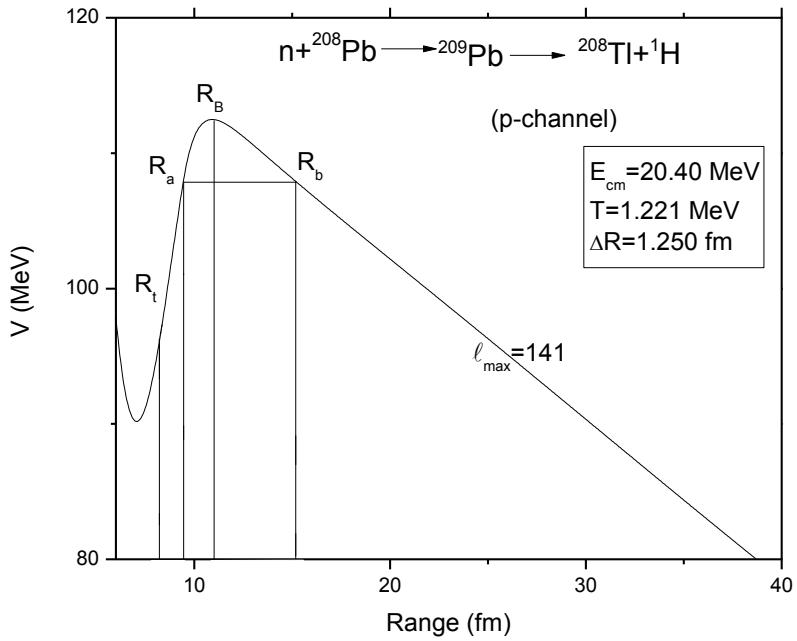

Fig. 2.1 Scattering potential of ^{208}Pb(n,p)^{208}Tl reaction at Ecm=20.40MeV.

DCM introduces a neck length parameter (ΔR) similar to that used in scission point and saddle point statistical fission model. The R_i are radius vectors which are also made temperature dependent and can be calculated as:

$$R_i(\alpha_i) = R_{0i}\left[1 + \sum_{\lambda} \beta_{\lambda i} Y_{\lambda}^{(0)}(\alpha_i)\right] \tag{2.17}$$

With $R_{0i}(T) = 1.28A_i^{1/3} - 0.76 + 0.8A_i^{-1/3} \times (1 + 0.0007T^2)$, (2.18)

2.5 References:

1. R. K. Gupta, M. Balasubraniam, C. Mazzocchi, M. La Commara and W. Scheid, Phys. Rev. C 64, 024601 (2002).
2. M. K. Sharma, R. K. Gupta and W. Scheid, J. Phys. G 26, L45 (2000).
3. R. K. Gupta, R. Kumar, N. K. Dhiman, M. Balasubraniam, W. Scheid and C. Beck, Phys. Rev. C 68, 014610 (2003).
4. M. Balasubraniam, R. Kumar, R. K. Gupta, C. Beck and W. Scheid, J. Phys. G 29, 2703 (2003): R. K. Gupta, M. Balasubraniam, R. Kumar, D. Singh and C. Beck, Nucl. Phys. A 738, 479c (2004).
5. B. B. Singh, M. K. Sharma, R. K. Gupta and W. Greiner, Int. J. Mod. Phys. E15, 699 (2006); B. B. Singh, M. K. Sharma and R. K. Gupta, Phys. Rev. C 77, 054613 (2008).
6. R. K. Gupta, S. K. Arun, R. Kumar and Niyti Int. Rev. Phys. (IREPHY) **2** 369 (2008).
7. M. K. Sharma, G. Sawhney, R. K. Gupta and W. Greiner, J. Phys. G: Nucl. Part. Phys. **38** 105101 (13pp) (2011).
8. K. Sandhu, M. K. Sharma and R. K. Gupta, Phys. Rev. C **85** 024604 (2012).
9. M. Kaur, R. Kumar and M. K. Sharma Phys. Rev. C **85** 014609 (2012); M. Kaur and M. K. Sharma Phys. Rev. C **85** 054605 (2012).
10. N. J. Davidson, S. S. Hsiao, J. Markram. H. G. Miller and Y. Tzeng, Nucl. Phys. A 570, 61c (1994).
11. P. A. Seeger, Nucl. Phys. 25, 1 (1961).
12. W. Myers and W. J. Swiatecki, Nucl. Phys. 81, 1 (1966).
13. N. Malhotra and R. K. Gupta, Phys. Rev. C 31, 1179 (1985).
14. Múnchow, D Hahn and W Scheid, Nucl. Phys. A 388, 381 (1982).
15. M. J. Rhoades-Brown, V E Oberacker, M Seiwert and W Greiner, Z. Phys. A 310,287 (1983).
16. C. Y. Wong, Phys. Rev. Lett. 31, 766 (1973).
17. R. Aroumougame and R K Gupta, J. Phys. G: 6, L155 (1980).
18. J. Blocki, J. Randrup, W. J. Swiatecki and C. F. Tsang, Ann. Phys. (NY) 105,427 (1977).
19. Deriyagin, Kolloid Z. 69, 155 (1934).

CHAPTER-3

Results and Discussions:

3.1 Introduction:

In this chapter we have applied dynamical cluster decay model (DCM) to neutron induced and heavy ion induced reactions using ^{204}Pb and ^{208}Pb targets. The neutron induced reactions are discussed in section-A and heavy ion induced reactions are discussed in section-B.

Section-A:

The neutron activation cross-sections have been measured using Pb isotopes over a wide range of energy 14-21 MeV [1]. A variety of neutron induced reactions of the type (n,n`γ), (n,2n), (n,3n), (n,α) and (n,p) etc have been investigated. In the present work we intend to use dynamical cluster decay model (DCM), to investigate the (n,2n) and (n,p) reactions on ^{204}Pb and ^{208}Pb along with some ^{20}Ne induced reactions on ^{208}Pb target. The calculations are done by including the deformations up to quadrupole (β_2) [2] with optimum orientation [3] approach and the experimental data is tested within the framework of dynamic cluster decay model (DCM) [4-8]. The following points are investigated:

1. The effect of level-density parameter is seen for ^{208}Pb (n,p) ^{208}Tl and ^{204}Pb (n,2n) ^{203}Pb reactions.
2. (n,p) and (n,2n) reactions of compound nuclei $^{205,\ 209}$Pb* are studied within energy range of 14-21 MeV in reference to data of [1].
3. Also, the fission cross-sections are calculated at 114.4 MeV for compound nucleus ^{228}U* formed in the reaction ^{20}Ne + ^{208}Pb in reference to data of [9].

As discussed in eq. 2.2, the excitation energy of compound nucleus E_{CN}^{*}, is related to temperature as:

$$E_{CN}^{*} = \frac{A}{a}T^{2} - T\ (MeV);$$

$where\ \frac{A}{a}\ is\ level\ density\ parameter\ with\ a\ in\ the\ range\ 9\ to\ 12.$

By taking level density parameter a=12, the comparision of (n,p) and (n,2n) reactions are done for isotopes $^{205,\ 209}$Pb* . The various values of the cross-sections are fitted in accordance with the experimental data by fitting *neck-length parameter, ΔR*. It is the only parameter of model which changes almost linearly with the variation of E_{cm}. Comparative study is done for compound nuclei $^{205,\ 209}$Pb* in terms of fragmentation potential (V_η), preformation probability

(P_0), cross-sections (σ) and penetrability (P) of the (n,p) and (n,2n) reactions. The data available for comparisons with us was of (n,p) reactions of ^{208}Pb and (n,2n) reactions of ^{204}Pb [1]. In order to have a harmonised study of (n,p) and (n,2n) reactions the target must be same and be investigated at similar incident energies. Therefore, we have done additional calculations for (n,p) reaction on ^{204}Pb and (n,2n) reaction on ^{208}Pb. For (n,p) reaction on ^{204}Pb we have taken same ΔR as that for ^{208}Pb target and similarly for (n,2n) reaction on ^{208}Pb, the ΔR values of ^{204}Pb target are used.

According to literature, [10] the level-density parameter plays very crucial role in deciding the cross-sections and various important parameters of the reactions. During the course of this work, the effect of level-density parameter has also been considered. It can be easily seen how the level-density parameter affects the cross-sections and fragmentation potential of (n,p) and (n,2n) reactions respectively on ^{208}Pb and ^{204}Pb targets.

The level density parameter is a crucial criterion for our calculations. Its value can be varied ranging from 9 to 12 in context of DCM.

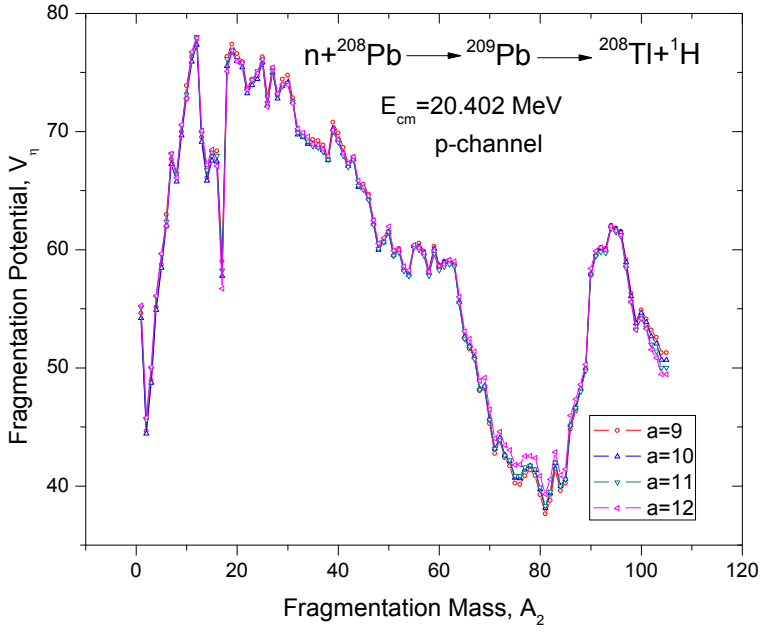

Fig. 3.1 Variation of fragmentation potential, V_η with fragment mass A_2 at different values of level density parameter 'a'.

A study shows that with increase in the value of a, there is a decrease in the value of ΔR. In context to the fragmentation potential shown in fig. 3.1, the conclusions drawn are that as the

value of ‘a’ inflates; there is an elevation in the values of fragmentation potential particularly in mass range A_2=70-90.

A closer view of fig. 3.1 can be helpful in distinguishing the variation as a function of level density parameter.

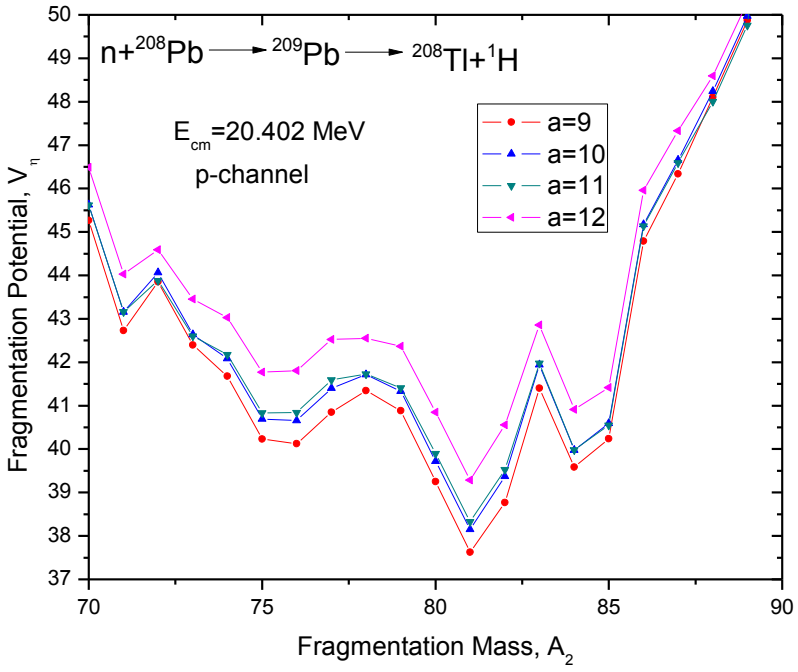

Fig. 3.2 Variation of fragmentation potential, V_η with fragment mass, A_2 at different values of level density parameter ‘a’ (magnified view).

In fig. 3.2, we tried to have a magnified view of the fragmentation plot at different values of level density parameter. The variation is depicted for fragment mass range A_2=70-90. Thus it can be seen clearly that as the value of level density parameter ‘a’ increases, the magnitude of fragmentation potential gets modified significantly but the structural variation remains unchanged. The modified fragmentation potential results in significant variation in decay cross-section. In case of (n,p) reactions of ^{208}Pb at E_{cm}=20.40 MeV, one can see in table 3.1 that for higher value of ‘a’, the same values of cross-sections (σ) are fitted nicely at lower values of *neck-length parameter, ‘ΔR’*. Thus, conclusively we can say that as the values of level-density parameter ‘a’ increases from 9 through 12, the value of ΔR decreases.

Table 3.1 DCM based cross-sections for ^{208}Pb(n,p)^{208}Tl reaction compared with experimental data taking different values of level density parameter 'a'.

E_{cm}(MeV)	A	T(MeV)	ΔR(fm)	ℓ_{max}	σ_{DCM}(mb)	σ_{exp}(mb)
20.40	09	1.054	1.315	138	8.46	8.1±0.5
20.40	10	1.112	1.295	139	8.50	8.1±0.5
20.40	11	1.168	1.278	140	8.25	8.1±0.5
20.40	12	1.221	1.250	141	7.75	8.1±0.5

In consequence, it is quite evident from the above table that as the values of 'a' increases, the values of reaction cross-sections also rises provided the other parameters like E_{cm}, ΔR etc. are kept constant. Hence, we conclude that level-density plays an eminent role in studying the reaction dynamics. Interesting aspect of table 3.1 is that the data of (n,p) reaction is fitted for all values of 'a' in the range 9 to 12. However, for (n,2n) reaction on ^{204}Pb the data could be fitted only with a=12, as shown in table 3.2. Analogously, we have also figured-out the effect of 'a' on cross-sections of ^{204}Pb (n,2n)^{203}Pb reactions. Interestingly, we were unable to fit the values of experimental cross-sections at lower values of 'a'. But as we take the value of 'a' equal to 12, we could get the desired cross-sections only at highest energy i.e. E_{cm}=20.29 MeV. The DCM based calculations under predict the data for (n,2n) reaction at lower incident energies. The DCM based cross-sections are compared with experimental data in table 3.2.

Table 3.2 DCM based cross-sections for ^{204}Pb(n,2n)^{203}Pb reaction compared with experimental data taking different values of level density parameter 'a'.

E_{cm}(MeV)	A	T(MeV)	ΔR(fm)	ℓ_{max}	σ_{DCM}(mb)	σ_{exp}(mb)
20.29	09	1.110	3.0	114	382	828±73
20.29	10	1.172	3.0	114	507	828±73
20.29	11	1.230	3.0	114	644	828±73
20.29	12	1.286	3.0	114	796	828±73

After the analysis of level-density parameter effects we intended to investigate other parameters that are indispensible for the survey of reaction dynamics of these nuclear

reactions and these include fragmentation potential and preformation probability etc. Attempts have been made to do a comparative study of fragmentation potentials for the reactions ^{208}Pb (n,p) ^{208}Tl with ^{204}Pb (n,p) ^{204}Tl and ^{208}Pb (n,2n) ^{207}Pb with ^{204}Pb (n,2n) ^{203}Pb reactions at comparable energy of E_{cm}~20.4 MeV. In the above mentioned reactions the fragmentation plots for compound nuclei ^{209}Pb* and ^{205}Pb* are compared for p and 2n reaction channels. The calculations are made using level density parameter, a=12. The values of ΔR, ℓ_{max}, corresponding temperatures (T) can be listed as under:

Table 3.3 The estimated cross-sections for ^{204}Pb(n,p)^{204}Tl and ^{208}Pb(n,2n)^{207}Pb along with fitted cross-sections for ^{208}Pb(n,p)^{208}Tl and ^{204}Pb(n,2n)^{203}Pb.

Reaction	E_{cm}(MeV)	T (MeV)	ΔR (fm)	ℓ_{max}	σ_{DCM}(mb)	σ_{exp}(mb)
^{208}Pb(n,p)^{208}Tl	20.40	1.221	1.250	141	7.75	8.10±0.5
^{204}Pb(n,p)^{204}Tl	20.40	1.289	1.250	134	14.60	-
^{208}Pb(n,2n)^{207}Pb	20.29	1.319	3.000	123	1130	-
^{204}Pb(n,2n)^{203}Pb	20.29	1.286	3.000	114	796	828±73

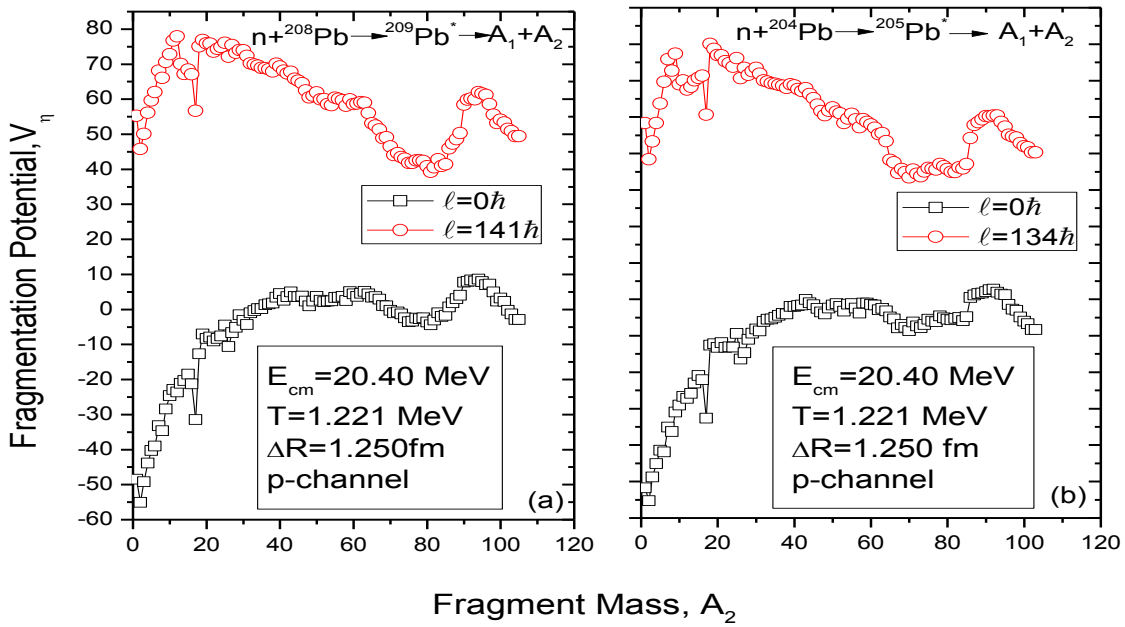

Fig.3.3 Variation of fragmentation potential, V_η with fragment mass,A_2 for ^{208}Pb(n,p)^{208}Tl and ^{204}Pb(n, p)^{204}Tl at E_{cm}=20.4 MeV.

The fragmentation potential for ^{208}Pb(n,p)^{208}Tl is shown in fig. 3.3(a) and for ^{204}Pb(n,p)^{204}Tl is shown in fig. 3.3(b).

The fig. 3.3(a) and fig. 3.3(b) demonstrate the variation of fragmentation potential (along Y-axis) as a function of fragment mass (along X-axis). Both figs. 3.3 (a) and 3.3 (b) are quite similar to each other at $\ell = \ell_{max}$, whereas some slight variation can be seen for $\ell=0$ case. From the fragmentation plots it can be inferred that lower the value of fragmentation potential; higher is the probability of decay of that fragment. At $\ell=0$ as well as at $\ell=\ell_{max}$, the dominating region in both the cases comprise of fragments in mass range from A_2=65 to 89 along with evaporation residues i.e. fragments with mass number $A_2 \leq 4$. This implies that the decay probabilities are high for these fragments.

Thus, one can say that the lower values of V_η correspond to higher decay possibilities. The comparisons of preformation probabilities of various fragments of the reactions ^{208}Pb (n,p) ^{208}Tl and ^{204}Pb (n,p) ^{204}Tl at comparable energies of E_{cm}~20.4 MeV is shown in fig. 3.4 (a) and 3.4 (b). In both the cases, the level density parameter is kept same i.e. a=12.

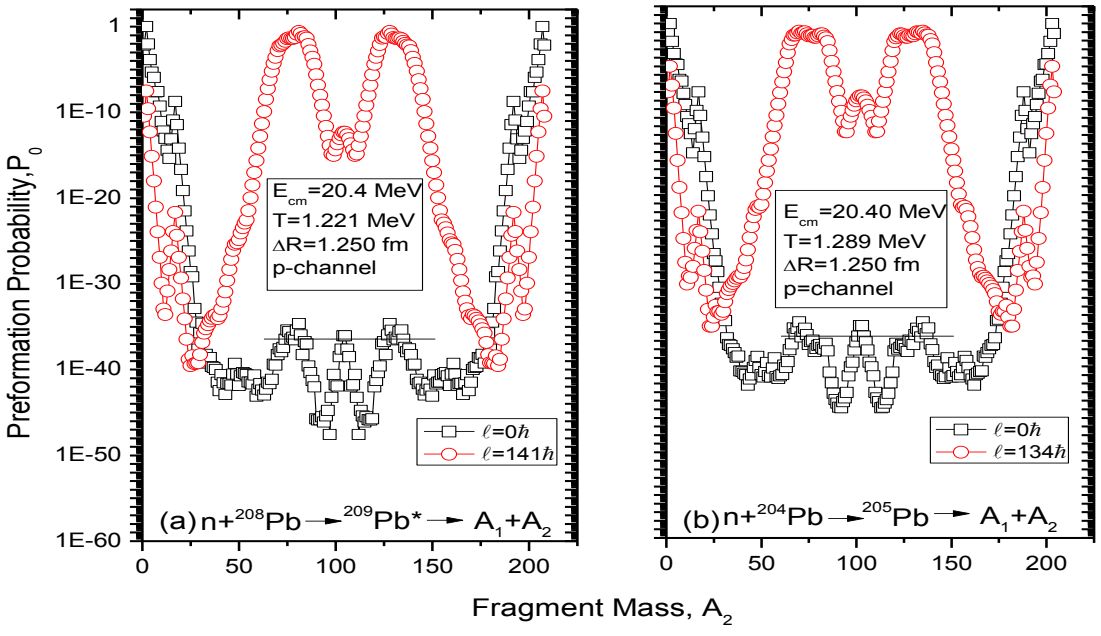

Fig. 3.4 Variation of preformation probability, P_0 with fragment mass, A_2 for ^{208}Pb (n,p) ^{208}Tl and ^{204}Pb (n,p) ^{204}Tl reaction at E_{cm}=20.4 MeV at $\ell=0$ and $\ell=\ell_{max}$.

The preformation probability, P_0 gives information about the structure of the compound nucleus. In fig. 3.4(a) and 3.4(b) the preformation probabilities are plotted (along Y-axis) against fragment mass (along X-axis). The comparative view of preformation patterns for p-channel reaction on ^{208}Pb and ^{204}Pb target enables us to conclude the underlying results.

- We have got asymmetric components of fission fragments in fig. 3.4 for (n,p) reactions. Although at ℓ=0, both symmetric and asymmetric components seem to be participating in fragmentation process.
- The second important point to be noted here is that as the value of angular momentum, ℓ goes up; the symmetric component starts disappearing. Thus, at $\ell=\ell_{max}$ the major portion towards cross-section is from asymmetric fission fragments. Here again some symmetric fission fragments are showing emergence but their contribution seems negligibly small.

Similar results can be achieved when we make comparative study of fragmentation potential plots and preformation probability plots for ^{208}Pb (n,2n) ^{207}Pb and ^{204}Pb (n,2n) ^{203}Pb reaction.

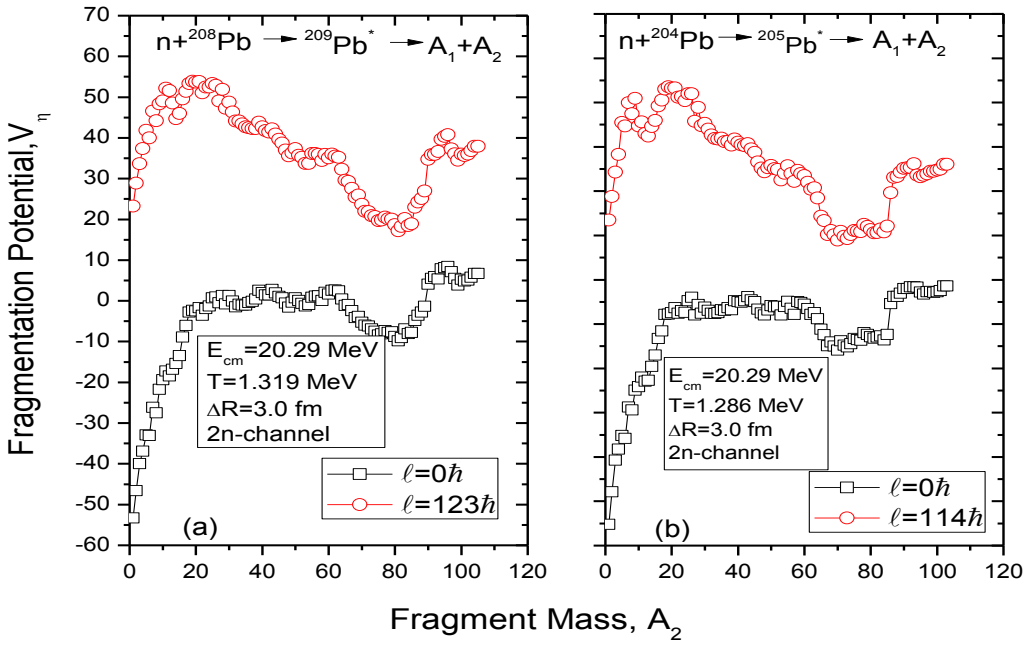

Fig.3.5 Variation of fragmentation potential, V_η with fragment mass, A_2 for ^{208}Pb (n,2n) ^{207}Pb and ^{204}Pb (n,2n) ^{203}Pb reaction at E_{cm}=20.29 MeV.

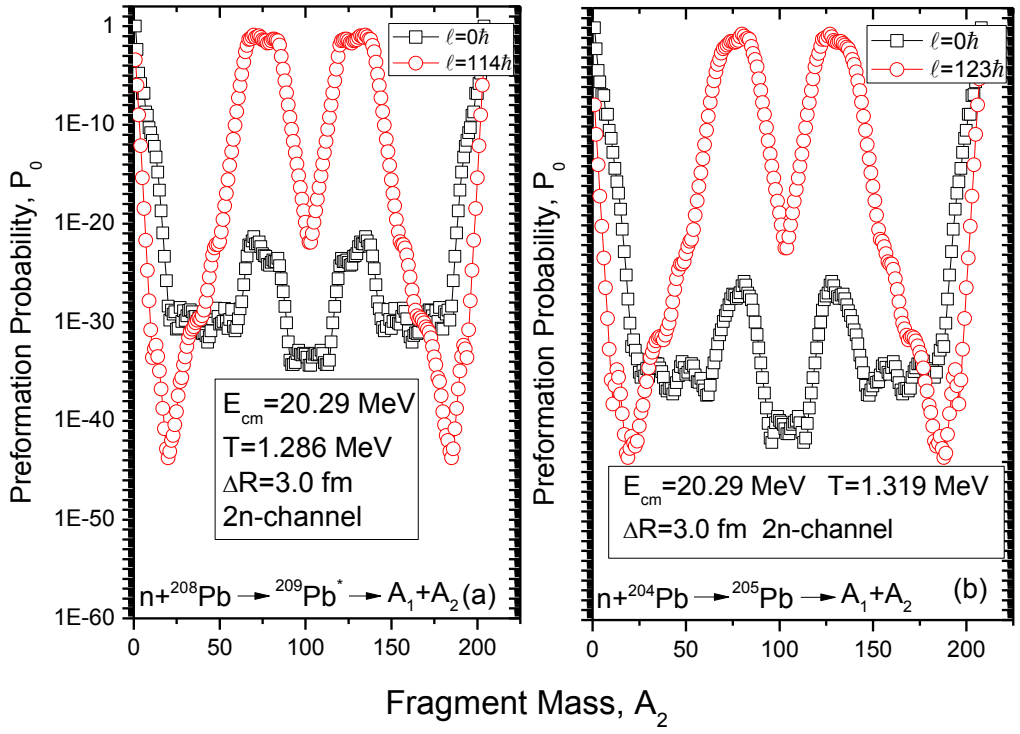

Fig. 3.6 Variation of preformation probability, P_0 with fragment mass, A_2 for ^{208}Pb (n,2n) ^{207}Pb and ^{204}Pb (n,2n) ^{203}Pb reaction at E_{cm}=20.29 MeV.

Thus it is clear from the aforementioned graphs that we have got similar fragmentation behaviour and preformation probability for ^{208}Pb (n,2n) ^{207}Pb and ^{204}Pb (n,2n) ^{203}Pb. Fig. 3.5 shows that here also the fragments ranging from A_2=65 to 89 have relatively higher decay possibilities with respect to neighbouring fragments, as their fragmentation potential is lower. Fig. 3.6 depicts the variation of preformation probability with fragment mass A_2. Here the preformation plots are asymmetric in nature. And this asymmetric behaviour is similar at both values of angular momentum i.e. ℓ=0 and $\ell=\ell_{max}$ unlike what is seen for (n,p) reactions where symmetric fragments also contribute at lower ℓ-values.

Furthermore, after analysing the various plots for these (n,p) and (n,2n) reactions, next comes the reaction cross-sections.The nuclear cross-section of a nucleus is used to characterize the probability that a nuclear reaction will occur. The concept of a nuclear cross section can be quantified physically in terms of "characteristic area" where a larger area means a larger probability of interaction. In our work under consideration, successful attempts have been made to fit the values of cross-sections for the reactions - ^{208}Pb (n,p) ^{208}Tl reaction using

neutron as projectile within energy range of 14-21 MeV. However, the data for ^{204}Pb(n,2n)^{203}Pb could be only fitted at higher energy. These results can be tabulated as:

Table 3.4 DCM based cross-sections compared with experimental data at different excitation energies, E^*_{CN} for reaction ^{208}Pb(n,p)^{208}Tl.

E^*_{CN}(MeV)	T (MeV)	ΔR (fm)	ℓ_{max}	σ_{DCM}(mb)	σ_{exp}(mb)
19.0774	1.076	0.950	160	0.885	0.95±0.22
20.5604	1.116	1.180	140	2.660	2.1±0.3
22.2024	1.158	1.210	141	4.140	4.2±0.4
23.5444	1.192	1.240	141	6.600	6.1±0.5
24.7404	1.221	1.250	141	7.750	8.1±0.5

A tidy correlation between our study and experimental data is evident from the graphs:

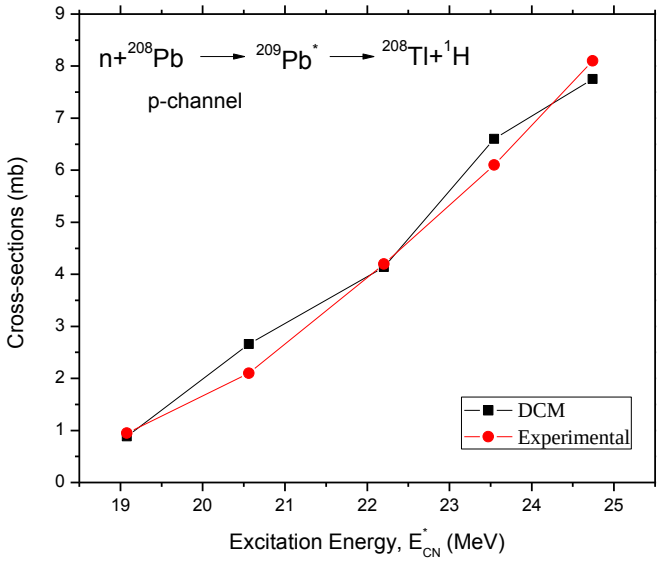

Fig.3.7 DCM based cross-sections and experimental data for (n,p) reaction of ^{208}Pb.

Section-B:

The above discussions are made for the study of p and 2n decay when ^{208}Pb and ^{204}Pb are incident upon by neutron beams within energy range 14-21 MeV [1]. In place of these neutron beams we can also use heavy-ion beams for the study of various reaction parameters. When heavy-ion beams are used then if the compound nucleus thus formed has light mass it will decay into LP's or IMF's. But if the compound nucleus is having heavy masses, then most probably its mode of decay will be fission. Just like that, here we have made ^{208}Pb to be incident upon by a beam of ^{20}Ne which leads to the formation of ^{228}U* which undergo fission because of its instability against centrifugal repulsions. Since $A^* \geq 200$, so our system will decay into a number of fission fragments [9].

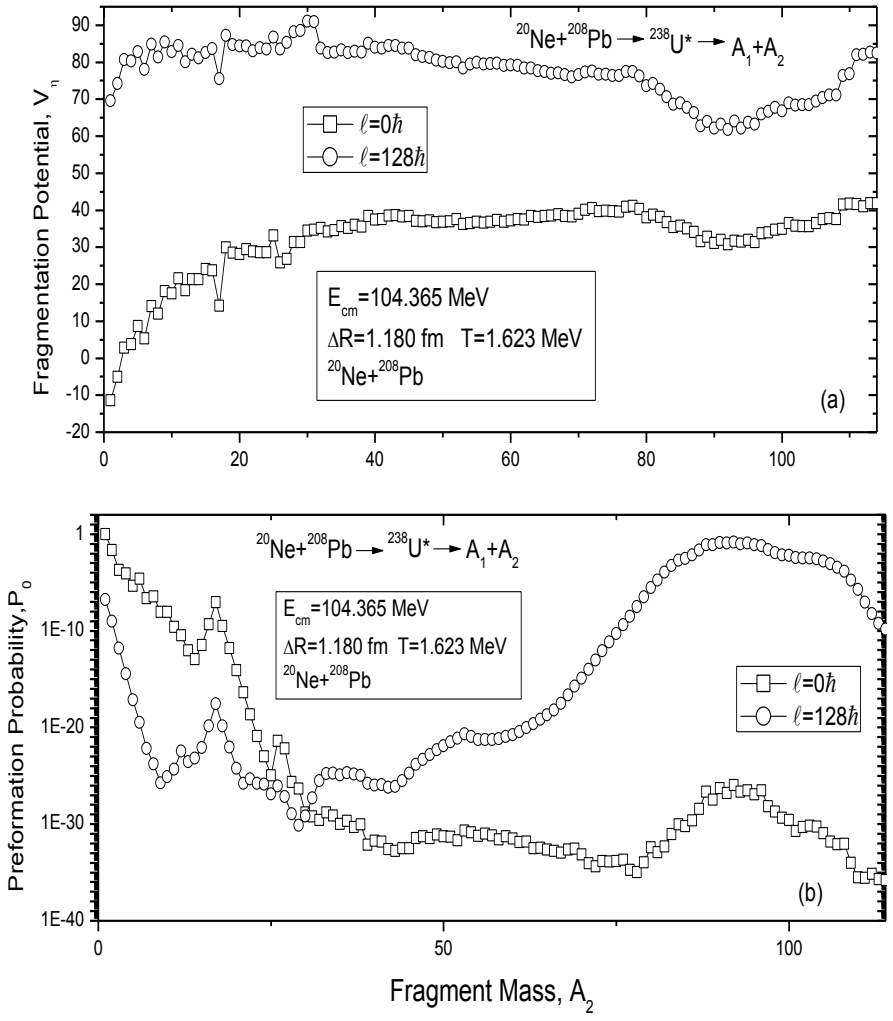

Fig. 3.8 (a) Fragmentation potential, Vη and (b) preformation probability, P_0 as a function of fragment mass, A_2 for ^{20}Ne + ^{208}Pb reaction.

This system is studied for fission E_{cm}=104.356 MeV and the reaction cross-sections for this reaction were fitted nicely by taking the values of neck-length parameter, ΔR=1.180fm using level density parameter, 'a' as 12 and ℓ_{max}=128. Thus here also we can study the fragmentation and preformation plots as shown respectively in the fig.3.8(a) and 3.8(b). In the fragmentation potential plot, as we already know that the lower values of V_η correspond to those fragments whose possibility of decay is more, thus, here the fragments corresponding to lower values of V_η are having mass numbers ranging from A_2=84 to 106. They are having higher decay possibilities. It is worth noting that the prominent fission fragments identified by DCM calculations are similar to the ones observed in [9].

About the preformation probability curve, the peak values on the curves correspond to those fragments who have lower values of V_η thereby indicating that they have higher decay possibilities. Along with the fragments having mass numbers from A_2=84 to 106, the complimentary fragments are also included in the cross-section calculations. It is worth noting that DCM based fission cross-sections 370mb compare nicely with the experimental data 382.8 mb.

3.2 Conclusions:

Conclusively, in this work an attempt is made to see how level density parameter affects the fragmentation path and consequently the reaction cross-sections. It is observed that a rise in the value of level density parameter causes a rise in the values of cross-sections and fragmentation potential. With an increase in 'a', there is an increase in the value of ℓ_{max} while the value of ΔR decreases. Then we investigated the fragmentation and preformation probability for the ^{208}Pb (n,p) ^{208}Tl and ^{204}Pb (n,2n) ^{203}Pb reactions. It is seen that the evaporation residues especially p and 2n respectively, and the fragments ranging from mass 65 to 89 correspond to lower values of V_η signifying that they have relatively high decay possibilities. In other words, such fragments have high values of preformation probabilities which shows that the probability of the decay of these fragments is much high as compared to the ones in their neighbourhood. Steering further, we have also calculated the reaction cross-sections for aforementioned reactions and our results fairly agree with experimental data for (n,p) reactions at all values of excitation energies E_{CN}^* and level density parameter, a. But on the other hand, for (n,2n) reactions the results are virtuous only at highest excitation energies, E_{CN}^* with 'a'=12. In addition to this, the heavy-ion induced reaction ^{20}Ne + ^{208}Pb is investigated to account for fission cross-sections. In the fission of $^{228}U^*$, it is seen that the

fragments having mass number from A_2=84 to 106 have high decay probability in agreement with experiment, such fragments have high contributions towards reaction cross-sections. These results adequately harmonize with the experimental data. So, we will synopsize by claiming that we have made successful attempts to account for (n,p) and heavy-ion induced reactions using ^{208}Pb as target, whereas (n,2n) reaction on ^{204}Pb couldn't be fully excercised. It will be of further interest to apply DCM for (n,n'γ), (n,3n) and (n,α) reactions using various heavy stable targets.

3.3 References:

1. V. Semkova *etal.* Phys. Rev. C 80 024610 (2009).
2. P. Möller, J. R. Nix, W. D. Myers and W.J. Swiatecki, At. Nucl. Data Tables 59, 185 (1995).
3. Raj K. Gupta, M. Balasubramaniam, Rajesh Kumar, Narinder Singh, Monika Manhas and W. Greiner J. Phys. G: Nucl. Part. Phys. 31 (2005) 631-644.
4. R. K. Gupta, S. K. Arun, R. Kumar and Niyti Int. Rev. Phys. (IREPHY) **2** 369 (2008).
5. B. B. Singh, M. K. Sharma and R. K. Gupta, Phys. Rev. C **77** 054613 (2008).
6. M. K. Sharma, G. Sawhney, R. K. Gupta and W. Greiner, J. Phys. G: Nucl. Part. Phys. **38** 105101 (13pp) (2011).
7. K. Sandhu, M. K. Sharma and R. K. Gupta, Phys. Rev. C **85** 024604 (2012).
8. M. Kaur, R. Kumar and M. K. Sharma Phys. Rev. C **85** 014609 (2012); M. Kaur and M. K. Sharma Phys. Rev. C **85** 054605 (2012).
9. R. Tripathi *etal* Phys. Rev. C, Vol. 69, 024613 (2004).
10. K. Banerjee *etal*. Phys. Rev. C, Vol. 85, 064310 (2012).